Journal of
Polymer Materials

Tech Science Press

Doi:10.32604/jpm.2025.060699

ARTICLE

Preparation of PVA/SA Interpenetrating Double Network Municipal Sludge Hydrogel and the Study of pH Response

Yu Huang[1,3], Tingting Dong[1], Xing Zhang[1], Shasha Xu[2], Xiaoyu Song[2], Zhaojun Wang[2], Mingyan Qin[1], Liwei Deng[1] and Yalin Li[1,2,*]

[1]School of Civil Engineering, Architecture and Environment, Hubei University of Technology, Wuhan, 430068, China
[2]School of College of Environmental and Biological Engineering, Henan University of Engineering, Zhengzhou, 451191, China
[3]National Engineering Research Center of Advanced Technology and Equipment for Water Environment Pollution Monitoring, Wuhan, 430068, China

*Corresponding Author: Yalin Li. Email: li_ya_lin@haue.edu.cn

Received: 07 November 2024; Accepted: 21 January 2025; Published: 27 March 2025

ABSTRACT: The rapid urbanization underscores the urgency of efficient treatment and resource utilization of municipal sludge for environmental conservation. To address this, a novel pH-responsive dual network polyvinyl alcohol/sodium alginate sludge hydrogel was devised by integrating municipal sludge with acrylic acid monomers, ammonium persulphate initiator, N, N'-methylene bisacrylamide crosslinking agent, reinforced by polyvinyl alcohol and sodium alginate through free radical cross-linking polymerization. The hydrogel's optimal formulation was identified by adjusting the monomer, crosslinking agent, and initiator dosage while assessing its swelling behavior across various pH environments. Results revealed excellent swelling capacity, notably exhibiting a remarkable swelling capacity of up to 7265.64% at pH 11.0, suggesting the hydrogel's potential in environmental remediation and innovative material design. This research presents a pioneering approach to harnessing municipal sludge and developing intelligent hydrogels, fostering sustainable resource management.

KEYWORDS: Municipal sludge; hydrogel; pH responsivity; response surface optimization

1 Introduction

The escalating industrialization and urbanization have led to a surge in domestic wastewater discharge, resulting in a corresponding increase in sludge production [1–3]. This sludge contains hazardous substances like heavy metals, organic pollutants, parasites, pathogens, and malodorous compounds, posing a significant threat to urban environmental cleanliness [4–6]. Globally, the volume of sludge generated is expected to reach 3 billion tons annually by 2025, highlighting the need for sustainable solutions across the world. In 2022, China's wastewater treatment capacity surpassed 216 million tons daily, generating over 100 million tons of sludge annually, including pipeline silt [7]. However, dwindling landfill space and closures have exacerbated the sludge disposal challenge. While China faces significant challenges, it's important to note that 60% of sludge worldwide remains untreated, contributing to environmental and health concerns [8]. The Chinese government has set ambitious targets for sludge treatment, aiming for over 90% harmless disposal by 2025 and full disposal by 2035 [9]. By the end of 2021, the rate of harmless disposal of urban sludge in China was about 64%, indicating that there is still a gap in reaching the 2025 target, emphasizing the urgency to explore innovative, nationally-suited sludge management strategies [10]. Traditional methods

like landfilling, incineration, and land utilization have limitations, prompting researchers to delve into new technologies. Innovative approaches such as anaerobic digestion, composting and resource recovery are being explored in a number of countries, and a number of international organizations, including the United Nations Environment Programme (UNEP), are advocating for a global framework for sustainable sludge management to address the global sludge crisis. However, the high cost of implementing new technologies and the lack of infrastructure in many developing regions pose significant barriers to achieving sustainable sludge management on a global scale. Among the emerging technologies, smart hydrogels are a promising solution for sludge disposal.

Hydrogels are advanced polymer materials with a three-dimensional network structure and exceptional water absorption capacity [11]. Due to their water absorption, hydrogels are now used in many applications, including wound dressings [12], agriculture [13], environmental remediation [14], nanotechnology [15], and drug delivery [16]. Intelligent hydrogels, an evolution of this technology, possess the unique ability to detect and respond to changes in the external environment, including pH, temperature, light, electricity, and magnetic fields [17]. The concept of intelligent hydrogels originated in 1975 when MIT researchers observed a polypropylene hydrogel undergoing reversible opacity changes with temperature fluctuations, indicating a phase transition in its polymer network. Since then, the field has attracted extensive research, exploring its diverse applications in drug delivery, molecular devices, and light-modulating materials [18–20]. As an emerging material, smart hydrogels contribute significantly to developing intelligent and eco-friendly soft materials, enhancing material efficiency, safety, and environmental sustainability [21]. Depending on their responsiveness, these hydrogels can be categorized into pH-sensitive, temperature-sensitive, electric field-sensitive, and magnetic-sensitive [22].

In recent years, significant progress has been made in the study of pH-responsive hydrogels, demonstrating their great potential for applications in the fields of drug delivery, environmental remediation and smart materials. Through a variety of synthetic strategies, such as one-pot method and crosslinker cross-linking, researchers have prepared hydrogels with various structural and functional properties. For example, Avais et al. used the reaction of branched polyethyleneimine (PEI) with an azetidine cross-linker to prepare a hydrogel that exhibited selective swelling behavior at close to physiological pH and was successfully applied to drug delivery systems [23]. Meanwhile, Li et al. synthesized a temperature and pH dual-responsive hydrogel through the synergistic interaction of sodium alginate, borax and carboxymethyl chitosan (CMCS), which demonstrated good water retention and antimicrobial properties for slow-release of fertilizers [24]. Wang et al. further expanded the field by developing a conductive hydrogel based on graphene oxide, which was applied to flexible sensors and logic gate design, achieving a smart material for sensing [25]. The innovative application of smart materials in the field of sensing was realized. In addition, pH-responsive hydrogels have also made important breakthroughs in performance regulation. By adjusting the cross-linking density and introducing functional groups, researchers have achieved precise regulation of hydrogel swelling, mechanical properties and drug release rate, etc. Agarwal et al. prepared a metal hydrogel with pH-responsiveness and multi-enzyme mimetic activity by self-assembly of adenylate (AMP) and cobalt chloride ($CoCl_2$) [26]. An et al. prepared a lignin hydrogel with pH responsiveness by introducing tertiary amino groups into lignin via a thiol-alkyne reaction, which provides a new direction for the application of hydrogels in the field of biomaterials [27]. In addition, several international studies have been devoted to the development of new smart hydrogel materials, such as carbon nanotube-enhanced ionic liquid bi-network conductive hydrogels [28] and flexible strain sensors prepared with the biomolecule sodium alginate [29], etc.

Traditional hydrogels face limitations in water absorption and mechanical property, necessitating modifications to enhance their swelling properties [30]. Although smart hydrogel technology shows great potential in sludge treatment, it still suffers from limitations such as high production cost, lack of stability, poor

biodegradability, and limited application scenarios. The aim of this study was to develop a pH-responsive smart hydrogel based on municipal sludge and to explore its potential application in sludge treatment. This hydrogel exhibits remarkable capabilities in selectively adsorbing and separating heavy metal ions, organic pollutants, and other contaminants from sludge, leveraging its unique swelling behavior and adjustable pore structure that responds to environmental pH changes. This targeted approach significantly enhances sludge treatment efficiency. Based on this, in this study, the pH-responsive poly(vinyl alcohol)/sodium alginate sludge hydrogel (PVA/SA sludge hydrogel, PSSH) was prepared by interpenetration of PVA and SA using municipal sludge as the research material, and by optimizing the hydrogel preparation process, the hydrogel material with excellent pH-responsive and adsorption properties was obtained to achieve effective adsorption and separation of heavy metal ions, organic pollutants, and other hazardous substances in the sludge and recovery and utilization of nutrients such as nitrogen and phosphorus.

2 Materials and Methods

2.1 Experimental Materials

The sludge utilized in this experiment originated from the primary dewatered sludge of a sewage treatment facility located in Xinzheng City, Zhengzhou and the inorganic components of the sludge mainly included SiO_2, Al_2O_3 and CaO, accounting for 23.10%, 11.60% and 2.13%, respectively. Upon retrieval, the sludge was promptly stored in a refrigerator at 4°C to preserve its integrity, and each batch was utilized within a span of 7 days to ensure consistency. For batches exceeding 7 days, fresh sludge was procured, and its fundamental properties were rigorously tested and recorded in Table 1. The relevant medicines required for the preparation of hydrogels including acrylic acid (AA), PVA, SA, ammonium persulphate (APS), N, N'-methylene bisacrylamide (MBA), the specific information of the drugs is shown in Table 2 [31], and the proportion of weight of the drugs used in the preparation of hydrogels is shown in Table 3; the chemicals required for the configuration of pH buffer including sodium bicarbonate, sodium hydroxide, potassium dihydrogen phosphate, disodium hydrogen phosphate, citric acid, ammonium chloride, ammonia, and potassium chloride, were all of analytical grade, ensuring the accuracy and reliability of the experimental results.

Table 1: Properties of sludge slurry

pH	Electrical conductivity (EC), us·cm^{-1}	Moisture content (MC), %	Total organic carbon (TOC), %
7.20–7.64	0.75–0.81	83.26–87.68	63.54–68.88

Table 2: The specific information of the experimental drugs

Experimental drug	Formula	Grand	Manufacturer
Acrylic acid (AA)	$C_3H_4O_2$	Analytical grade	Tianjin Kemiou Chemical Reagent Co., Ltd., Tianjin, China
Polyvinyl alcohol (PVA)	$(C_2H_4O)_x$	Analytical grade	Shanghai Yi En Chemical Technology Co., Ltd., Shanghai, China
Sodium alginate (SA)	$C_6H_7NaO_6$	Analytical grade	Sinopharm Chemical Reagent Co., Ltd., Shanghai, China

(Continued)

Table 2 (continued)

Experimental drug	Formula	Grand	Manufacturer
Ammonium persulphate (APS)	$(NH_4)_2S_2O_8$	Analytical grade	Tianjin Fengchuan Chemical Reagent Co., Ltd., Tianjin, China
N, N′-methylene bisacrylamide (MBA)	NNMBA	Analytical grade	Shanghai Aladdin Biochemical Technology Co., Ltd., Shanghai, China

Table 3: The weight proportions of all the materials used in the preparation of the hydrogel

Material	Weight, g
PVA	1.0000
SA	0.0539
AA	3.0000
APS	0.1000
MBA	0.1500

2.2 Preparation Method and Principle of PSSH

2.2.1 Preparation Method of PSSH

To prepare the sludge slurry, a precise amount of municipal sludge was measured and combined with deionized water in a 1:50 mass ratio. This mixture was then thoroughly pulverized using a wall breaker, resulting in a uniform sludge slurry. From this slurry, 50 mL was accurately measured and transferred into a beaker. The beaker containing the sludge slurry was placed on a constant temperature water bath stirrer and preheated at 70°C for 15 min to ensure uniform temperature. Following preheating, monomers AA was introduced into the beaker, and after 5 min, PVA was added to the reaction system. After another 5 min of stirring, a 0.067 mol/L SA was incorporated. Ten minutes later, the initiator APS was added to the beaker, followed by the addition of the crosslinking agent MBA after a brief wait of 1 min. The reaction was maintained at a constant temperature within the water bath throughout this process, forming a yellow-brown hydrogel solid termed PSSH. The entire procedure is schematically illustrated in Fig. 1.

2.2.2 Preparation Principle of PSSH

As depicted in Fig. 2, the sludge slurry undergoes decomposition under heating conditions when triggered by the initiator APS, yielding sulfate radicals ($SO_4^{-}\cdot$) [32]. These radicals, characterized by their unpaired electrons, exhibit high reactivity and can engage in reactions with AA molecules by abstracting hydrogen atoms adjacent to the carbon-carbon double bond (C=C), thereby generating new radicals. These newly formed radicals continue the chain growth process by reacting with additional AA molecules [33]. Concurrently, the presence of APS facilitates the crosslinking of active sites present on the polymeric chains of PVA and SA, leading to the formation of an interpenetrating network structure (IPN) [34]. This ongoing process encourages the successive polymerization of monomer molecules, resulting in the emergence of long-chain polymers [35]. Furthermore, the crosslinking agent MBA engages in a covalent crosslinking reaction with the unsaturated double bonds of AA, forming more stable covalent bonds and establishing crosslinking sites. These sites connect various polymer chains through carbon-carbon (C-C) or carbon-oxygen (C-O) single bonds, ultimately constructing a three-dimensional network structure at the molecular level [36].

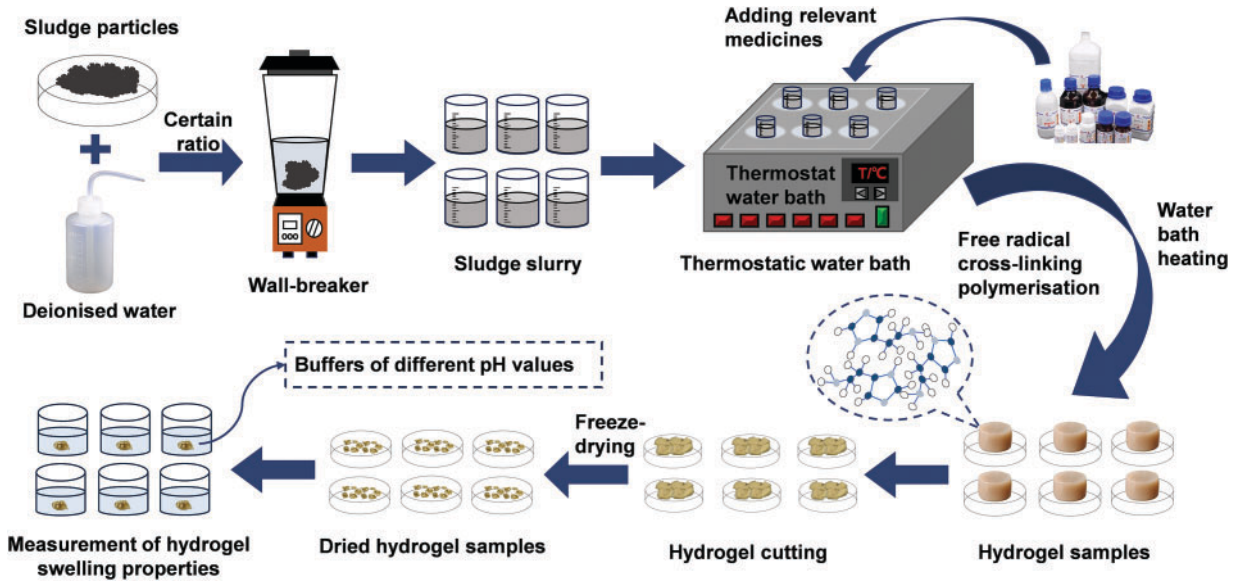

Figure 1: Schematic diagram of the PSSH preparation process

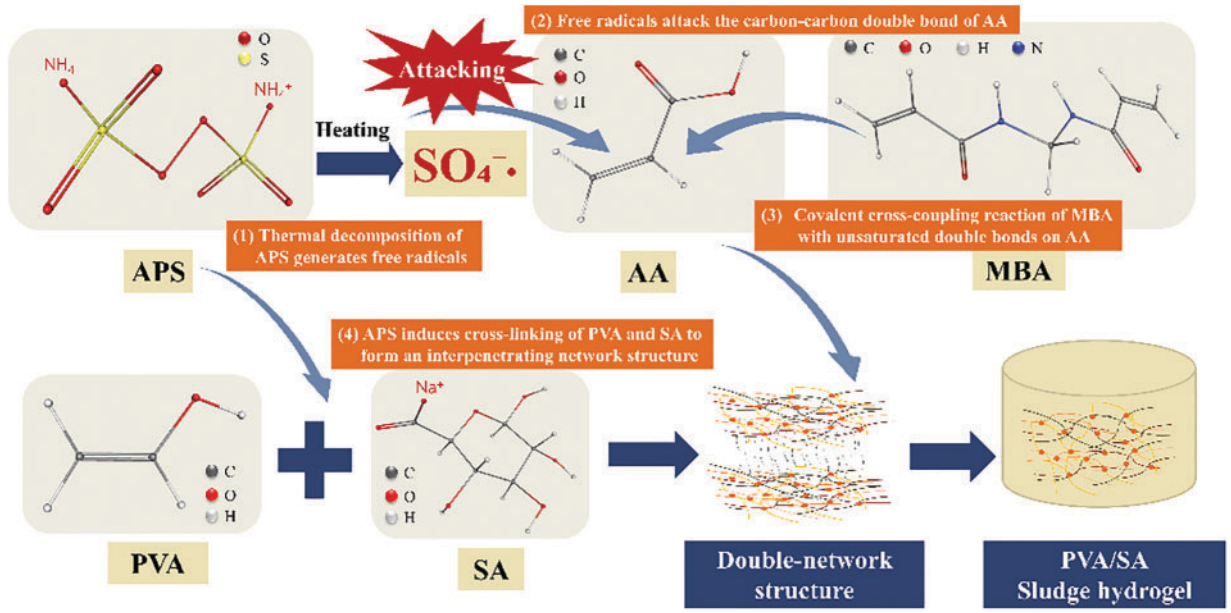

Figure 2: Schematic diagram of PSSH preparation principle

2.3 Determination of Swelling Capacity of PSSH

The prepared PSSH was subjected to vacuum freeze-drying until it reached a dry state. Subsequently, a predetermined mass of the dried hydrogel was placed in a beaker containing a pH buffer solution, allowing it to absorb water and swell. After a period of time, the hydrogel was removed from the solution, and any excess water on its surface was gently removed using absorbent paper. The mass of the hydrated hydrogel was then measured. This process was repeated until the hydrogel was completely broken. The swelling capacity

of the hydrogel was subsequently calculated using the equation provided in (1) [37].

$$S_c = \frac{W_s - W_0}{W_0} \quad (1)$$

where S_c is the swelling capacity of hydrogel, %; W_s is the mass of hydrogel after swelling and water absorption, g; W_0 is the mass of dry hydrogel before swelling, g.

2.4 Materials Characterizations

The dry hydrogel samples prepared under the best conditions were ground into powder and passed through a 140-mesh sieve. XRD was conducted by D8 ADVANCE X-ray diffractometer of Bruker, Germany, with a scanning range of 2θ = 10°–80°. FT-IR determination was performed with KBr tablet compression method in the range of 4000–500 cm^{-1} with the Fourier infrared spectrometer Nicolet 6700 of Thermo Fisher Company. The hydrogel samples prepared under the best conditions were freeze-dried and then determined by SEM with liquid nitrogen embrittlement with a Sigma300+ Oxford energy spectrum scanning electron microscope (Zeiss).

3 Results and Discussion

3.1 Effects of Different Factors on the Swelling Capacity of PSSH

A series of one-way experiments were used to systematically investigate the effects of different factors on the swelling characteristics of PSSH hydrogels. In all the experiments, the mass ratio of sludge to deionized water was always kept at 1:50, and 50 mL of sludge slurry was placed into a magnetic thermostatic water bath stirrer with the temperature of the water bath set at 70°C. The optimal dosages of AA, PVA, SA, APS, and MBA were determined from the preliminary experiments to be 3.0 mL, 1.00 g, 8.0 mL, 0.10 g, and 0.20 g. Subsequently, the swelling behavior of the hydrogels was fully explored by varying individual factors while keeping other factors constant. This involved adjusting the pH of the pH buffer to 8.0, 9.0, 10.0, 11.0, 12.0, and 13.0 in an experiment to assess the responsiveness of the hydrogel to pH. And by changing a single variable, i.e., control AA (2.0, 2.5, 3.0, 3.5, 4.0, 4.5 mL), PVA (0.25, 0.50, 0.75, 1. 00, 1.25, 1.50 g), SA (2.0, 4.0, 6.0, 8.0, 10.0, 12.0 mL), APS (0.05, 0.10, 0.15, 0. 20, 0.25, 0.30 g), and MBA (0.10, 0.15, 0.20, 0.25, 0.30, 0.35 g) to analyze the effect of different dosages of the drugs on the swelling capacity of the hydrogel, and the swelling data obtained are shown in Figs. 3–8.

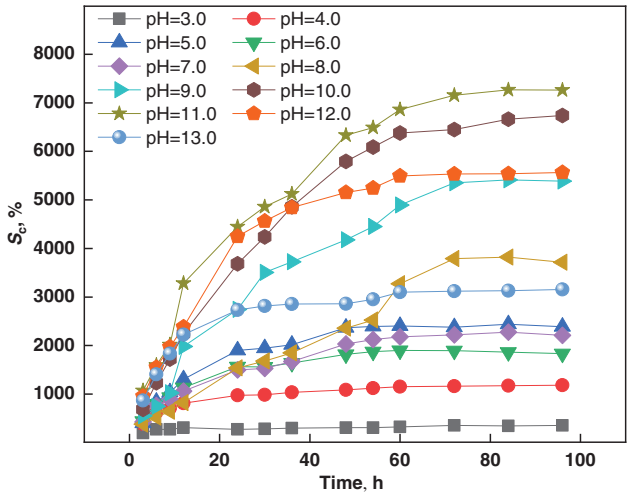

Figure 3: Effect of different pH values on the swelling capacity of PSSH

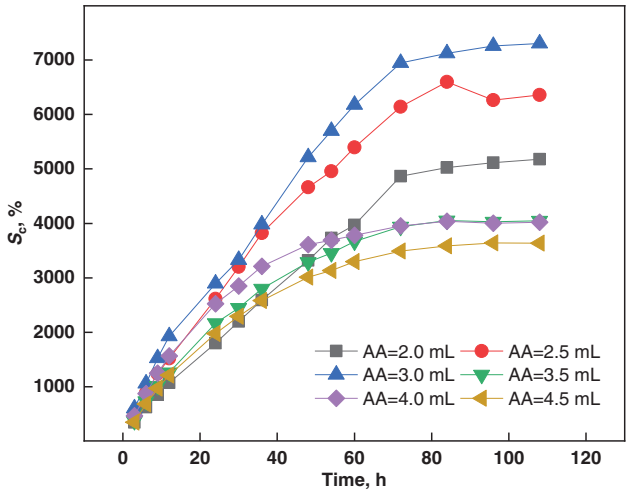

Figure 4: Effect of AA dosage on swelling capacity of PSSH

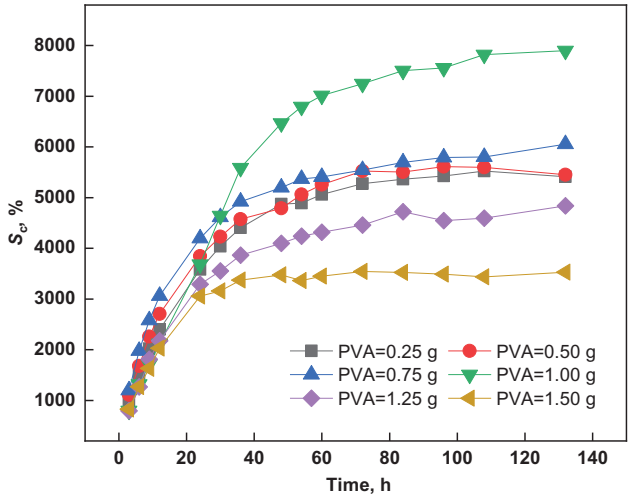

Figure 5: Effect of PVA dosage on swelling capacity of PSSH

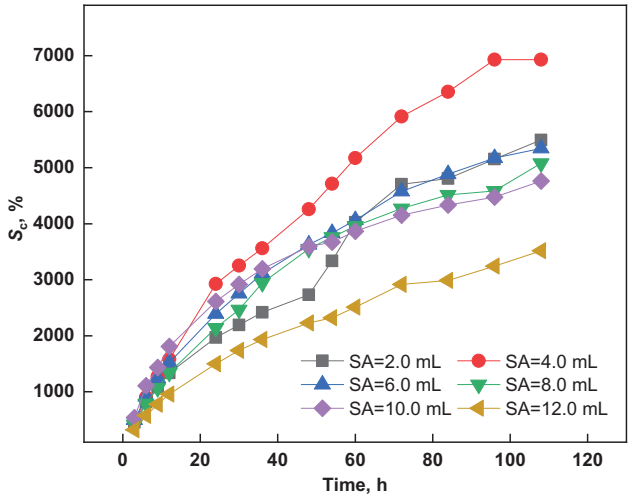

Figure 6: Effect of SA dosage on the swelling capacity of PSSH

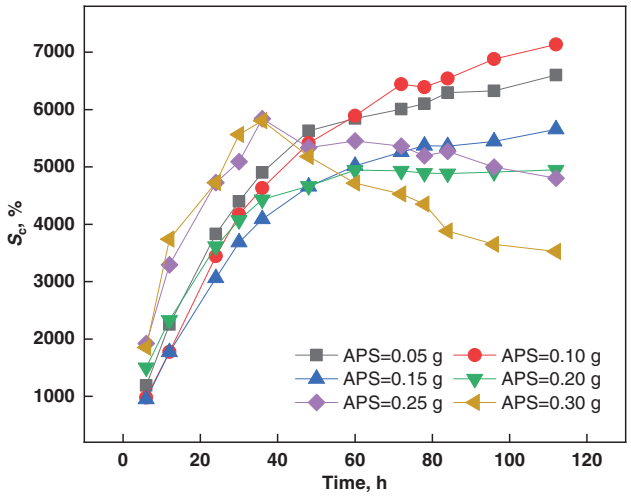

Figure 7: Effect of APS dosage on swelling capacity of PSSH

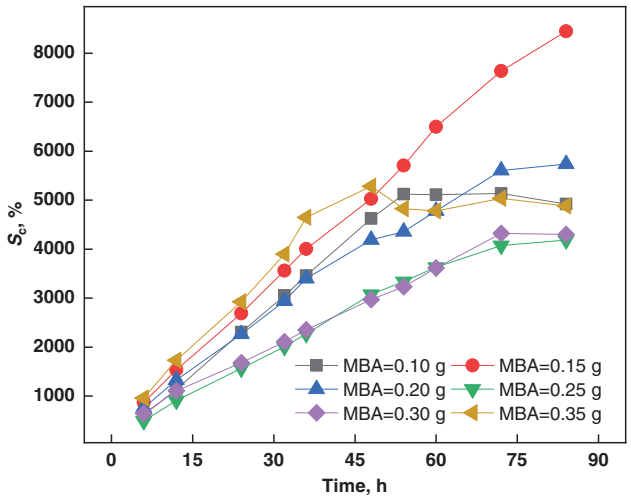

Figure 8: Effect of MBA dosage on swelling capacity of PSSH

3.1.1 Effect of Different pH on the Swelling Capacity of PSSH

As depicted in Fig. 3 and Table 4, the swelling behavior of PSSH in varying pH buffers exhibits an initial rise followed by stabilization. Notably, at the pH of 11.0, the hydrogel's swelling capacity attains a peak of 7265.64%, suggesting a heightened sensitivity of its crosslinking points to alkaline environments. This alkaline pH (11.0) partially disrupts the crosslinking structures, resulting in a looser polymer network [38]. Furthermore, the presence of ionizable acidic groups (carboxyl groups, for instance) within the hydrogels undergoes deprotonation under alkaline conditions, acquiring a negative charge. This charge repulsion among similar charges causes the polymer chains to unfold, thereby facilitating the solubilization of the hydrogel and enhancing its swelling capacity [39,40].

Table 4: Swelling data of PSSH in different pH buffers

pH	S_c, %
3.0	346.90
4.0	1172.82
5.0	2440.78
6.0	1864.47
7.0	2275.67
8.0	3822.20
9.0	5410.58
10.0	6662.48
11.0	7265.64
12.0	5541.67
13.0	3129.56

3.1.2 Effect of AA Dosage on the Swelling Capacity of PSSH

As depicted in Fig. 4, the swelling capacity of PSSH in a pH 11.0 buffer solution exhibited a distinct trend of initially increasing and subsequently decreasing with the escalation of AA monomer dosage. Specifically, the hydrogel's swelling capacity peaked at 7304.02% when the AA dosage was precisely 3.0 mL. This phenomenon can be attributed to the role of AA in the polymerization process. AA, being a monomer with reactive double bonds, undergoes polymerization reactions in an alkaline environment to form polyacrylic acid (PAA) [41]. In this pH 11.0 buffer, the carboxyl groups of PAA partially or fully dissociate, acquiring a negative charge. This negative charge enhances the interaction between the polymer chain and water molecules, resulting in swelling [42]. However, further increments in AA dosage beyond 3.0 mL leads to a decline in swelling capacity. This is due to an increase in chain transfer reactions during polymerization, yielding polymers with lower molecular weights that exhibit reduced swelling capacity. Additionally, excess AA can disrupt the uniformity of the polymerization reaction, leading to the formation of an inhomogeneous hydrogel network. This inhomogeneity can create localized regions within the hydrogel that are overly compact, ultimately hindering the overall swelling capacity of the material.

3.1.3 Effect of PVA Dosage on the Swelling Capacity of PSSH

As shown in Fig. 5, with the increase of PVA dosage, the swelling capacity of PSSH in buffer solution with pH 11.0 showed a trend of first rising and then falling. When the PVA dosage was 1.00 g, the swelling capacity of the hydrogel was up to 7897.71%, which is because PVA molecules contain many hydroxyl groups. These hydroxyl groups can form hydrogen bonds with water molecules, giving PVA excellent water absorption and retention [43–47]. Under alkaline conditions, the hydroxyl groups in PVA molecules will partially dissociate and form negative charges, increasing the interaction with water molecules and leading to the swelling and swelling of the PVA molecular chains, affecting the swelling capacity of hydrogels. However, too much PVA leads to higher hydrogel crosslinking density, restricts the movement of polymer chains, and reduces the ability of water to enter the hydrogel network, reducing the hydrogel's swelling capacity [48].

3.1.4 Effect of SA Dosage on the Swelling Capacity of PSSH

As depicted in Fig. 6, the swelling behavior of PSSH in a pH 11.0 buffer solution initially escalated and subsequently declined with an increase in SA concentration. Notably, the hydrogel attained its peak swelling

ratio of 6928.55% at an SA dosage of 4.0 mL. This phenomenon can be attributed to the influence of SA dosage on the hydrogel's crosslink density. An optimal SA amount fosters a moderately cross-linked hydrogel network, enhancing water absorption and retention, thereby boosting swelling capacity [49]. Conversely, excessive SA results in a densely cross-linked network that hinders water penetration, ultimately diminishing the swelling capacity [50,51].

3.1.5 Effect of APS Dosage on Swelling Capacity of PSSH

As evident from Fig. 7, the swelling capacity of PSSH in a pH 11.0 buffer solution exhibited a biphasic trend, initially escalating and subsequently declining with increasing APS dosage. At an APS dosage of 0.10 g, the hydrogel achieved its peak swelling ratio of 7132.74%. This behavior stems from APS's varying stability across different pH levels [52]; it is more stable under acidic conditions and decomposes faster in alkaline environments. The quantity of free radicals generated by APS decomposition directly correlates with the number of crosslinking points during polymerization, thereby influencing the hydrogel's crosslinking density [53]. The decomposition process of APS is outlined in Eqs. (2) and (3). An optimal APS amount facilitates the generation of sufficient free radicals to enhance monomer polymerization and foster the development of a stable hydrogel network [54]. However, excessive APS can lead to a rapid polymerization reaction, resulting in an uneven hydrogel network that hinders swelling capacity [55]. Additionally, excessive swelling or mechanical stress can compromise the hydrogel network's integrity, leading to a significant drop in its swelling capacity.

$$(NH_4)_2S_2O_8 \rightarrow 2NH_4^+ + 2SO_4^{2-} \tag{2}$$

$$2SO_4^{2-} \rightarrow 2SO_4^- \cdot + 2e^- \tag{3}$$

3.1.6 Effect of MBA Dosage on Swelling Capacity of PSSH

As depicted in Fig. 8, the swelling capacity of PSSH in a pH 11.0 buffer solution initially increased and then decreased with the escalation of MBA crosslinking agent dosage. At an MBA dosage of 0.15 g, the hydrogel achieved its peak swelling capacity of 8445.33%. This trend arises due to the ionization of abundant functional groups (e.g., hydroxyl and carboxyl) within the sludge-based hydrogel, generating negative charges that repel each other, thereby expanding the hydrogel volume (i.e., swelling) [56]. However, under alkaline conditions, MBA's hydroxyl groups can form hydrogen bonds with the hydrogel's hydroxyl, carboxyl, and other functional groups, enhancing the hydrogel's stability [57–60]. Consequently, as MBA dosage increases, the enhanced hydrogen bonding effect diminishes the hydrogel's swelling capacity [61].

3.2 RSM Surface Response Optimization

Utilizing the findings from the one-factor experiment, a Box-Behnken response surface methodology was employed to further optimize the swelling capacity of PSSH in pH 5.0, 7.0, and 11.0 buffer solutions. Specifically, three key variables, monomer AA dosage (A), PVA dosage (B), and SA dosage (C), were identified as factors to be varied at three different levels. This three-factor, three-level experimental design aimed to determine the optimal process conditions for PSSH preparation. The experimental factors and their respective levels were outlined in Table 5, while the experimental program and the resulting data were presented in Table 6. The ultimate goal was to achieve optimal swelling capacity of PSSH across the three different pH buffer conditions.

Table 5: RSM experimental factors and levels design

Factor	Level		
	–1	0	1
A: AA dosage, mL	2.50	3.00	3.50
B: PVA dosage, g	0.75	1.00	1.25
C: SA dosage, mL	2.00	4.00	6.00

Table 6: RSM experimental program and results

Number	AA dosage, mL	PVA dosage, g	SA dosage, mL	S_c, % (pH = 5.0)	S_c, % (pH = 7.0)	S_c, % (pH = 11.0)
1	3.0	1.00	4.0	1697.41	3912.77	6478.51
2	3.0	1.00	4.0	1577.32	3571.36	6576.32
3	2.5	1.00	2.0	1360.30	1729.71	4666.88
4	3.0	1.00	4.0	1608.27	3597.78	6340.06
5	3.0	1.25	2.0	1115.76	2577.43	4156.76
6	3.5	1.00	2.0	1311.01	1697.38	4639.03
7	2.5	0.75	4.0	1105.12	1895.54	5320.90
8	3.0	0.75	2.0	1055.81	2628.37	4212.51
9	3.0	1.00	4.0	1563.77	3663.88	6173.30
10	2.5	1.25	4.0	1241.24	2062.00	4282.10
11	3.0	0.75	6.0	1049.28	2535.97	5138.90
12	3.0	1.25	6.0	1102.32	2610.24	3265.48
13	3.5	1.00	6.0	1208.31	1721.82	4500.00
14	3.5	0.75	4.0	1200.68	1915.03	4595.34
15	3.0	1.00	4.0	1683.46	4206.27	6834.80
16	2.5	1.00	6.0	1256.93	1613.42	7030.35
17	3.5	1.25	4.0	1123.80	2031.54	4389.81

Based on the data in Table 6, PSSH performs best in a buffer with a pH of 11.0. To analyze and fit this data, a second-order model analysis was used, and a regression equation was derived. Furthermore, a quadratic regression surface equation was established based on this analysis, as shown in Eq. (4).

$$S_c = -37150.09 + 14581.84A + 34186.38B + 3452.09C + 2266.54AB - 125.63AC - 908.84BC - 2785.82A^2 - 19393.70B^2 - 268.77C^2 \quad (4)$$

The results of analysis of variance (ANOVA) are presented in Table 7; from the data analysis, the F-value of the model is 33.96, $p < 0.0001$, indicating that the response value of the model is very significantly affected by this experimental factor [62]. The correlation adjustment coefficient of the model, R^2_{Adj}, was 0.9488, and the correlation prediction coefficient, R^2_{Pred}, was 0.8476, in which $R^2_{Adj} - R^2_{Pred} < 0.2$ and the C.V.% was 3.89%, which is less than 10%, indicating that this model has a high degree of accuracy, suggesting that the experimental results can be analyzed and predicted with this regression surface equation [63,64].

Table 7: Response polygon ANOVA results

Source	Sum of squares	Df	Mean square	*F*-value	*p*-value	
Model	1.71×10^7	9	1.90×10^6	33.96	<0.0001	Significant
A	2.72×10^5	1	2.72×10^5	4.88	0.0629	
B	1.03×10^6	1	1.03×10^6	18.49	0.0036	
C	8420.78	1	8420.78	0.1509	0.7092	
AB	3.21×10^5	1	3.21×10^5	5.75	0.0476	
AC	63126.56	1	63126.56	1.13	0.3229	
BC	8.26×10^5	1	8.26×10^5	14.80	0.0063	
A^2	2.04×10^6	1	2.04×10^6	36.59	0.0005	
B^2	6.19×10^6	1	6.19×10^6	110.83	<0.0001	
C^2	4.87×10^6	1	4.87×10^6	87.19	<0.0001	
Residual	3.91×10^5	7	55813.87			
Lack of fit	1.42×10^5	3	47295.99	0.7604	0.5721	Not significant
Pure error	2.49×10^5	4	62202.28			
Cor total	1.75×10^7	16				

The software generated the corresponding 3D response surface and contour plots, as shown in Fig. 9. The response surface was saddle-shaped, and the contour lines showed an oval shape, indicating a significant interaction between the two factors [65].

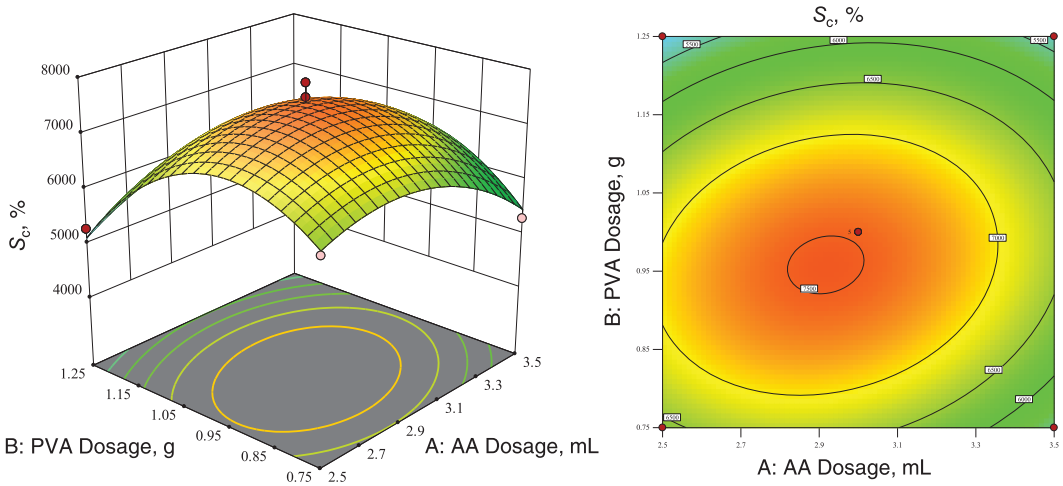

Figure 9: (Continued)

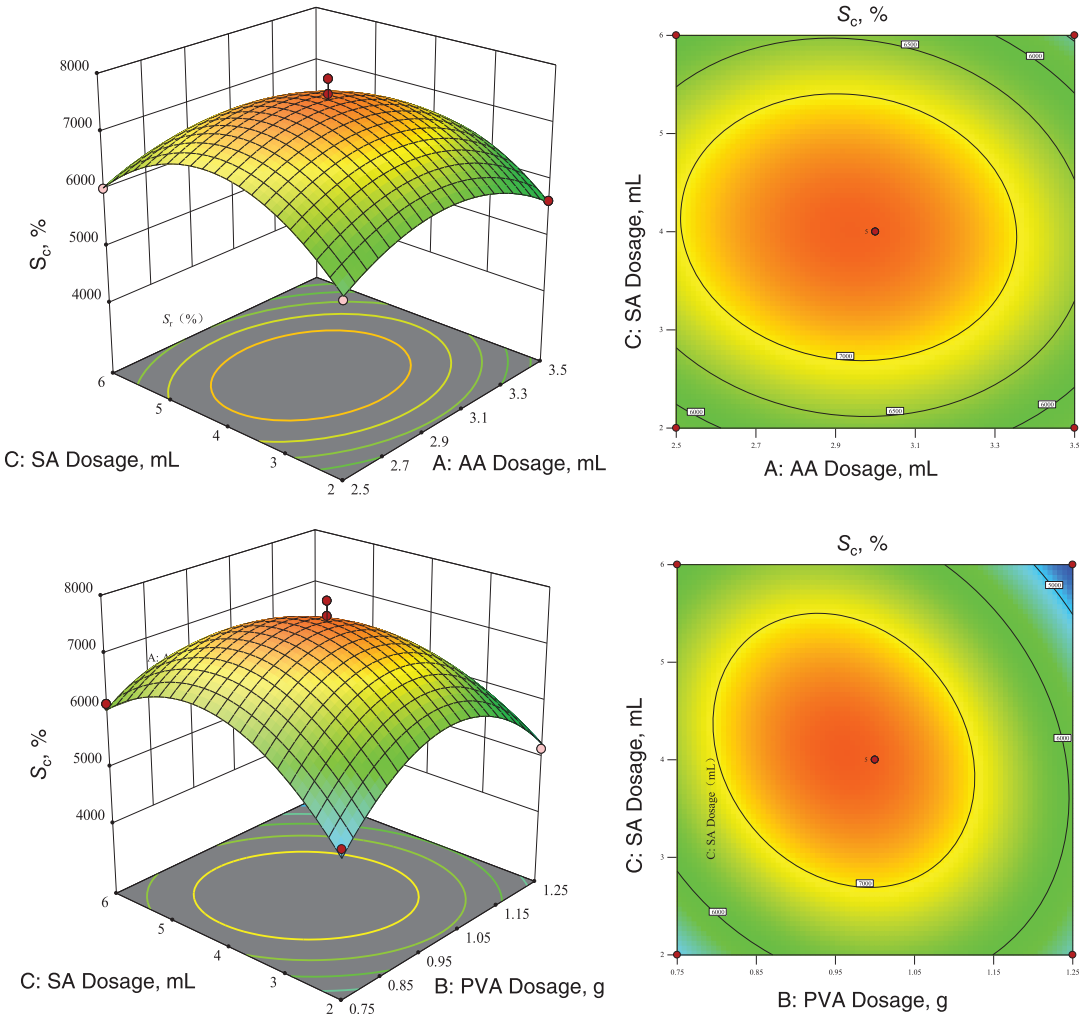

Figure 9: Three-dimensional response surface plots and two-dimensional contour plots of optimal dissolution capacity

3.3 Validation Experiment Results and Analysis

In order to verify the reliability of the experimental results, according to the optimized experiments using the software to select three groups of experiments to verify the analysis, the experimental results are shown in Table 8.

Table 8: Optimization verification experiment results

AA dosage, mL	PVA dosage, g	SA dosage, mL	S_c, %	
			Projected value	Actual value
2.742	0.981	3.597	7351.84	7609.79
2.500	0.750	4.000	6399.05	6762.48
3.000	1.000	4.000	7480.60	7261.56

As shown in Table 8, the predicted values are in good agreement with the actual values, and under the optimal conditions of prediction, i.e., the dosage of AA is 2.742 mL, the dosage of PVA is 0.981 g, and the dosage of SA solution is 3.597 mL, the prediction of S_c is 7351.84%, and the relative error compared with the predicted value is 3.51% < 5%, which indicates the prediction model can truly and accurately reflect the influence of each factor on the S_c value.

3.4 Characterization of PSSH

3.4.1 X-Ray Diffraction Analysis

As depicted in Fig. 10, SiO_2 crystallization diffraction peaks located at 2θ = 21.10°, 2θ = 26.68°, 2θ = 39.57°, and 2θ = 68.26° in the SH diffraction pattern, with the most vigorous intensity at 2θ = 26.68°, and the peaks corresponded to (101) crystalline surfaces. After the addition of PVA and SA, the intensity of SiO_2 crystallization diffraction peaks of PSSH became weaker, which could be analyzed as the polymer formed or the network physically adsorbed, due to the PVA and SA encapsulating the SiO_2 particles. The amorphous peaks of PSSH were higher than those of SH, which indicated that the crystallinity of PSSH increased further, and that the PVA and SA were in an amorphous form stabilized in the hydrogel and uniformly dispersed [66].

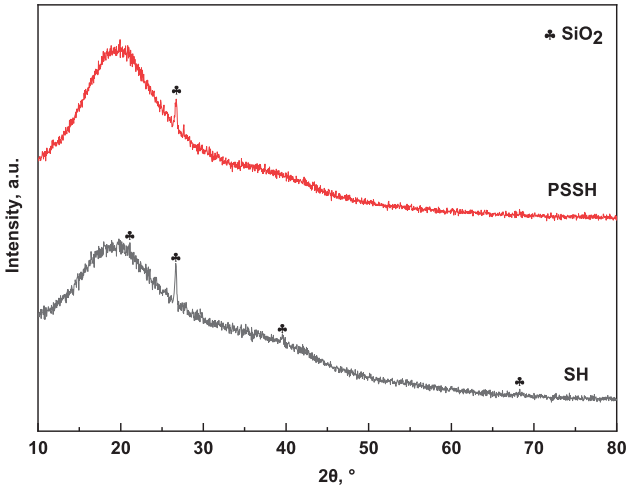

Figure 10: XRD patterns of PSSH and SH

3.4.2 Fourier Ransform Infrared Analysis

As depicted in Fig. 11, the infrared spectrum of the sludge hydrogel reveals a prominent carbonyl (C=O) stretching vibration peak at 1720 cm^{-1}, a characteristic hallmark of carbonyl-containing organic compounds, confirming the presence of such moieties within the hydrogel matrix. Additionally, the presence of Si-O stretching and bending vibration peaks at 1090 and 610 cm^{-1}, respectively, indicates the composition of the sludge material. In contrast, the PSSH infrared spectrum exhibits distinct C-H stretching and C-O stretching vibration peaks at 2948 and 1091 cm^{-1}, respectively. Notably, the strong carbonyl (C=O) stretching vibration peak at 1720 cm^{-1} arises from the esterification between PVA and SA components, providing evidence of their successful integration. Furthermore, the phosphate functional group absorption peak at 800 cm^{-1} verifies the complete reaction between PVA, SA, and the sludge. The significant appearance of COO- symmetric and asymmetric stretching vibration peaks at 1451 and 1540 cm^{-1}, respectively, underscores the successful modification of the hydrogel structure by PVA and SA, reinforcing the chemical interactions within the PSSH system [67]. The significant appearance of COO- symmetric and asymmetric stretching vibration peaks at

1451 and 1540 cm^{-1}, respectively, underscores the successful modification of the hydrogel structure by PVA and SA, reinforcing the chemical interactions within the PSSH system [67].

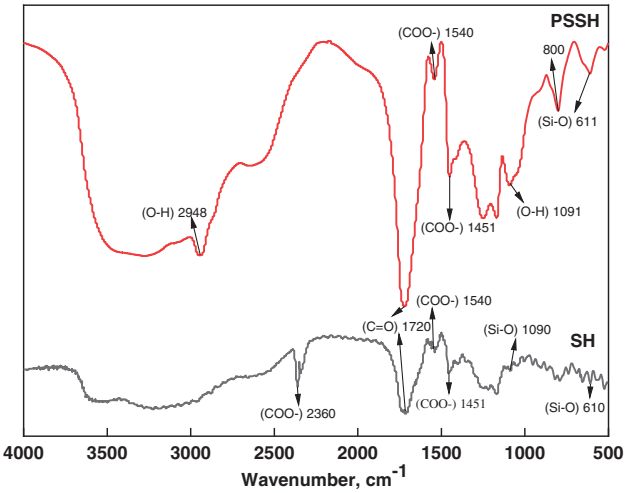

Figure 11: FT-IR patterns of PSSH and SH

3.4.3 Scanning Electron Microscopy Analysis

Fig. 12a,b illustrate the presence of SiO_2 particles adhering to the surface of the sludge hydrogel (SH), corroborating the XRD findings. The hydrogel interior lacks a discernible network structure, exhibiting numerous folds and an irregular morphology. In contrast, Fig. 12c reveals a pronounced double network structure within the PSSH hydrogel after the incorporation of PVA and SA. This double network, featuring intricately intertwined layers resembling a honeycomb pattern, signifies the successful formation of a dual-network architecture through the interpenetration of PVA and SA. This unique structure enhances the porosity and interconnectedness of the hydrogel, thereby augmenting its water absorption and retention capabilities, enabling it to undergo significant swelling upon hydration. Additionally, Fig. 12d showcases the crosslinking structure within the hydrogel, indicative of chemical reactions between PVA, SA, and specific components (e.g., metal ions) present in the sludge. These reactions generate chemical crosslinking points, which subsequently link polymer chains to construct a robust three-dimensional network structure [68].

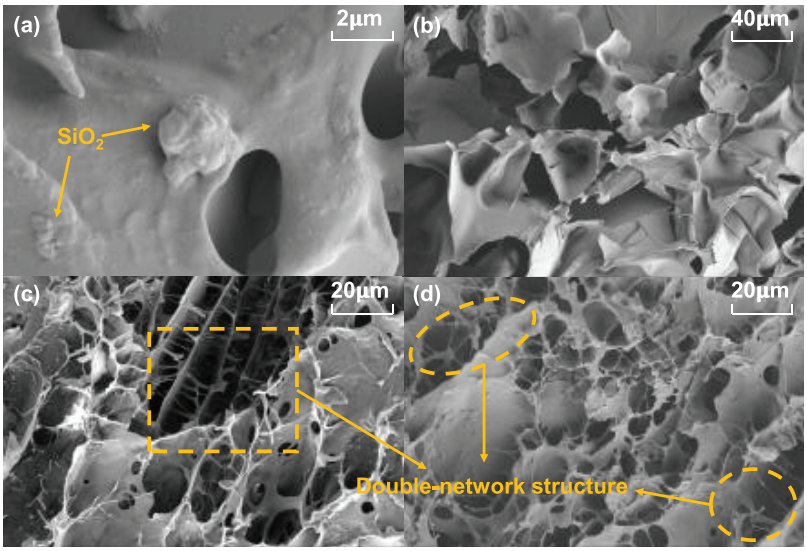

Figure 12: SEM image of SH and PSSH((a) (b) SH; (c) (d) PSSH)

4 Conclusions

In this manuscript, the pH-responsive PSSH was prepared from municipal sludge by interpenetration, and the optimal solution for the preparation of the hydrogel was determined by measuring the swelling capacity of the hydrogel in different pH buffers and exploring the effects of different preparation parameters on the pH-responsiveness of the hydrogel. On this basis, RSM optimization experiments further obtained the optimal preparation parameters. The PSSH prepared under the optimal condition parameters were characterized in various ways to investigate the material composition and morphological structure, and the conclusions drawn during the study are as follows:

1) In this study, a novel pH-responsive PSSH was successfully prepared by combining PVA and SA with municipal sludge via free radical cross-linking polymerization, which showed a high dissolution rate of 7351.84% under alkaline conditions (pH 11.0). The optimization and characterization of the PSSH revealed that the amounts of AA, PVA and SA had significant effects on the chemical structure and physical properties of the PSSH, which conferred pH-responsive properties, hydrophilicity and cross-linking network structure, respectively.

2) PSSH still faces challenges such as scalability, mechanical strength, stability and cost-effectiveness in practical applications, and further research and development is needed to optimize the preparation methods, improve the material properties and explore its practical applications in areas such as environmental treatment, wastewater treatment and resource recovery. Despite these limitations, PSSH is a promising method for sludge treatment and resource utilization. Its pH-responsive characteristics and ability to selectively adsorb and separate pollutants offer potential application areas for environmental remediation, wastewater treatment and resource recovery. Further research and development work is necessary to address the identified challenges and realize the full potential of PSSH to contribute to a more sustainable and environmentally friendly future.

Acknowledgement: The authors would like to extend our heartfelt gratitude to all those who have supported and assisted us in completing this paper.

Funding Statement: This research was funded by the Hubei Provincial Key Scientific Research Project on Water Resources "Study on the Distribution and Characteristics of Sediment Siltation in the Key Waters of Zhanghe Reservoir (HBSLKY202302)"; Wuhan Municipal Bureau of Science and Technology 2023 Knowledge and Innovation Special Project, "Research on key technology for fine traceability of total phosphorus in urban lakes in Wuhan" (No. 2023020201010119); and the National Visiting Scholar Program for Key Young Teachers of Central and Western Universities, and the Ministry of Education (19042); Science and Technology Tackling Projects in Henan Province in 2025 (Research on key technology for removing microdust from the surface of photovoltaic power generation panels by spray coating with high-efficiency hydrogel coatings prepared from multi-source solid wastes).

Author Contributions: The authors confirm contribution to the paper as follows: Conceptualization: Yu Huang and Yalin Li; methodology: Tingting Dong; formal analysis: Tingting Dong and Xing Zhang; investigation: Yu Huang, Yalin Li, Tingting Dong and Xing Zhang; resources: Yu Huang and Tingting Dong; data curation: Yu Huang and Yalin Li; writing—original draft preparation: Tingting Dong; writing—review and editing: Yu Huang, Yalin Li, Tingting Dong, Xing Zhang, Zhaojun Wang, Shasha Xu, Xiaoyu Song, Mingyan Qin and Liwei Deng; visualization: Tingting Dong and Xing Zhang; supervision: Yalin Li. All authors reviewed the results and approved the final version of the manuscript.

Availability of Data and Materials: The data that support the findings of this study are available from the corresponding author upon reasonable request.

Ethics Approval: The research does not involve the study of humans, animals, medical records and/or human tissue and teeth.

Conflicts of Interest: The authors declare no conflicts of interest to report regarding the present study.

Abbreviations

PVA	Polyvinyl alcohol
SA	Sodium alginate
PSSH	polyvinyl alcohol/sodium alginate sludge hydrogel
AA	Acrylic acid
APS	Ammonium persulphate
MBA	N, N'-methylene bisacrylamide
EC	Electrical conductivity
MC	Moisture content
TOC	Total organic carbon
SH	Sludge hydrogel
IPN	Interpenetrating network structure
RSM	Response surface methodology
ANOVA	Analysis of variance
XRD	X-ray diffraction
FT-IR	Fourier transform infrared
SEM	Scanning electron microscopy

References

1. Chen R, Ma X, Yu Z, Chen L, Chen X, Qin Z. Study on synchronous immobilization technology of heavy metals and hydrolyzed nitrogen during pyrolysis of sewage sludge. J Environ Chem Eng. 2021;9(5):106079. doi:10.1016/j.jece.2021.106079.

2. Geng H, Xu Y, Zheng L, Gong H, Dai L, Dai X. An overview of removing heavy metals from sewage sludge: achievements and perspectives. Environ Pollut. 2020;266(1):115375. doi:10.1016/j.envpol.2020.115375.
3. Rao B, Zhu Y, Yu M, Lu XL, Wan YJ, Huang G, et al. Highdry dewatering of sludge based on different pretreatment conditions. Process Saf Environ. 2019;122(2):288–97. doi:10.1016/j.psep.2018.12.018.
4. Li B, Ding S, Fan H, Ren Y. Experimental investigation into the effect of pyrolysis on chemical forms of heavy metals in sewage sludge biochar (SSB), with brief ecological risk assessment. Materials. 2021;14(2):447. doi:10.3390/ma14020447.
5. Liu L, Huang L, Huang R, Lin H, Wang D. Immobilization of heavy metals in biochar derived from co-pyrolysis of sewage sludge and calcium sulfate. J Hazard Mater. 2021;403(629):123648. doi:10.1016/j.jhazmat.2020.123648.
6. Zhou X, Zhang X, Zhang Z, Liu Y. Full nitration-denitration versus partial nitration-denitration-anammox for treating high-strength ammonium-rich organic wastewater. Bioresour Technol. 2018;261(5):379–84. doi:10.1016/j.biortech.2018.04.049.
7. Wei L, Zhu F, Li Q, Xue C, Xia X, Yu H, et al. Development, current state and future trends of sludge management in China: based on exploratory data and CO_2-equivaient emissions analysis. Environ Int. 2020;144(3):106093. doi:10.1016/j.envint.2020.106093.
8. Jones ER, Van Vliet MT, Qadir M, Bierkens MF. Country-level and gridded estimates of wastewater production, collection, treatment and reuse. Earth Syst Sci Data. 2021;13(2):237–54. doi:10.5194/essd-13-237-2021.
9. Ma M, Duan W, Huang X, Zeng D, Hu L, Gui W, et al. Application of calcium peroxide in promoting resource recovery from municipal sludge: a review. Chemosphere. 2024;354(6):141704. doi:10.1016/j.chemosphere.2024.141704.
10. Lu JY, Wang XM, Liu HQ, Yu HQ, Li WW. Optimizing operation of municipal wastewater treatment plants in China: the remaining barriers and future implications. Environ Int. 2019;129:273–78. doi:10.1016/j.envint.2019.05.057.
11. Yazdi MK, Vatanpour V, Taghizadeh A, Taghizadeh M, Ganjali MR, Munir MT, et al. Hydrogel membranes: a review. Mat Sci Eng C. 2020;114:111023. doi:10.1016/j.msec.2020.111023.
12. Xu M, Miao Y, Yu J, Zhang L. Physiologically-regulated adhesion of hydrogels for wound dressing. Adv Mater Interfaces. 2021;8(20):2101131. doi:10.1002/admi.202101131.
13. Uysal Y, Doğaroğlu ZG, Makas MN, Çaylali Z. Boosting water retention in agriculture: vine biochar-doped hydrogels' swelling and germination effects. Glob Chall. 2024;8(5):2300254. doi:10.1002/gch2.202300254.
14. Li D, Zhan W, Zuo W, Li L, Zhang J, Cai G, et al. Elastic, tough and switchable swelling hydrogels with high entanglements and low crosslinks for water remediation. Chem Eng J. 2022;450(15):138417. doi:10.1016/j.cej.2022.138417.
15. Wang R, Cheng C, Wang H, Wang D. Swollen hydrogel nanotechnology: advanced applications of the rudimentary swelling properties of hydrogels. ChemPhysMater. 2024;3(4):357–75. doi:10.1016/j.chphma.2024.07.006.
16. Park SY, Kim SY, Kang JH, Kim HS, Shin US. Design of thermoresponsive hydrogels by controlling the chemistry and imprinting of drug molecules within the hydrogel for enhanced loading and smart delivery of drugs. Mol Syst Des Eng. 2021;6(4):286–92. doi:10.1039/D0ME00097C.
17. Ding M, Jing L, Yang H, Machnicki CE, Fu X, Li K, et al. Multifunctional soft machines based on stimuli-responsive hydrogels: from freestanding hydrogels to smart integrated systems. Mater Today Adv. 2020;8:100088. doi:10.1016/j.mtadv.2020.100088.
18. Yang S, Liu Z, Pan Y, Guan J, Yang P, Asel M. A review of research progress on the performance of intelligent polymer gel. Molecules. 2023;28(10):4246. doi:10.3390/molecules28104246.
19. Li J, Zhang Y, Zhu L, Chen K, Li X, Xu W. Smart nucleic acid hydrogels with high stimuli-responsiveness in biomedical fields. Int J Mol Sci. 2022;23(3):1068. doi:10.3390/ijms23031068.
20. Ejeromedoghene O, Omoniyi AO, Akor E, Alowakennu M, Samson KA, Abesa S, et al. Progress in stimuli-responsive hydrogel composites for digital technologies. Appl Mater Today. 2024;37:102088. doi:10.1016/j.apmt.2024.102088.
21. Zou F, Xu J, Yuan L, Zhang Q, Jiang L. Recent progress on smart hydrogels for biomedicine and bioelectronics. Biosurf Biotribol. 2022;8(3):212–24. doi:10.1049/bsb2.12046.

22. Mehta P, Sharma M, Devi M. Hydrogels: an overview of its classifications, properties, and applications. J Mech Behav Biomed Mater. 2023;147(1):106145. doi:10.1016/j.jmbbm.2023.106145.
23. Avais M, Chattopadhyay S. Waterborne pH responsive hydrogels: synthesis, characterization and selective pH responsive behavior around physiological pH. Polymer. 2019;180(2):121701. doi:10.1016/j.polymer.2019.121701.
24. Li L, Bai G, Gu WJ, Niu CH, Feng YL, Wei Z, et al. Boronic ester bonds hydrogel with temperature and pH responsiveness for controlled release fertilizer. Ind Crops Prod. 2024;221:119336. doi:10.1016/j.indcrop.2024.119336.
25. Wang T, Zhang X, Wang ZC, Zhu XZ, Liu J, Min X, et al. Smart composite hydrogels with pH-responsiveness and electrical conductivity for flexible sensors and logic gates. Polymers. 2019;11(10):1564. doi:10.3390/polym11101564.
26. Agarwal V, Varshney N, Singh S, Kumar N, Chakraborty A, Sharma B, et al. Cobalt-adenosine monophosphate supramolecular hydrogel with pH-responsive multi-nanozymatic activity. ACS Appl Bio Mater. 2023;6(11):5018–29. doi:10.1021/acsabm.3c00719.
27. An L, Chen J, Heo JW, Kim JW, Mo Jeong H, Youn DH, et al. Preparation of pH-responsive lignin via a thiol-yne reaction and its application in hydrogel. J Wood Chem Technol. 2022;42(6):445–55. doi:10.1080/02773813.2022.2120898.
28. Han Y, Li Y, Liu Y, Alsubaie AS, El-Bahy SM, Qiu H, et al. Carbon nanotube reinforced ionic liquid dual network conductive hydrogels: leveraging the potential of biomacromolecule sodium alginate for flexible strain sensors. Int J Biol Macromol. 2024;282(23):137123. doi:10.1016/j.ijbiomac.2024.137123.
29. Liu Y, Jiang D, Wu Z, Jiang B, Xu Q. Highly conductive and sensitive acrylamide-modified carboxymethyl cellulose/polyvinyl alcohol composite hydrogels for flexible sensors. Sens Actuator A Phys. 2024;370(22):115258. doi:10.1016/j.sna.2024.115258.
30. Karoyo AH, Wilson LD. A review on the design and hydration properties of natural polymer-based hydrogels. Materials. 2021;14(5):1095. doi:10.3390/ma14051095.
31. Makhado E, Pandey S, Modibane KD, Kang M, Hato MJ. Sequestration of methylene blue dye using sodium alginate poly(acrylic acid)@ZnO hydrogel nanocomposite: kinetic, isotherm, and thermodynamic investigations. Int J Biol Macromol. 2020;162:60–73. doi:10.1016/j.ijbiomac.2020.06.143.
32. Li YL, Huang Y, Liu L, Liu HZ, He HY, Lu DX, et al. Nano-CaO_2 promotes the release of carbon sources from municipal sludge and the preparation of double-network hydrogels with high swelling ratios. J Renew Mater. 2023;11(3):1237–53. doi:10.32604/jrm.2022.022972.
33. Khan Y, Bashir S, Hina M, Ramesh S, Ramesh K, Lahiri I. Effect of salt concentration on poly (acrylic acid) hydrogel electrolytes and their applications in supercapacitor. J Electrochem Soc. 2020;167(10):100524. doi:10.1149/1945-7111/ab992a.
34. Koul V, Mohamed R, Kuckling D, Adler HJP, Choudhary V. Interpenetrating polymer network (IPN) nanogels based on gelatin and poly(acrylic acid) by inverse miniemulsion technique: synthesis and characterization. Colloids Surf B Biointerfaces. 2011;83(2):204–13. doi:10.1016/j.colsurfb.2010.11.007.
35. Cheng WM, Hu XM, Zhao YY, Wu MY, Hu ZX, Yu XT. Preparation and swelling properties of poly(acrylic acid-co-acrylamide) composite hydrogels. e-Polymers. 2017;17(1):95–106. doi:10.1515/epoly-2016-0250.
36. Huang H, Dong Z, Ren X, Jia B, Li G, Zhou S, et al. High-strength hydrogels: fabrication, reinforcement mechanisms, and applications. Nano Res. 2023;16(2):3475–515. doi:10.1007/s12274-022-5129-1.
37. Zhang K, Feng W, Jin C. Protocol efficiently measuring the swelling rate of hydrogels. MethodsX. 2020;7(2015):100779. doi:10.1016/j.mex.2019.100779.
38. Orakdogen N. Investigation of mechanical and thermodynamic properties of pH-sensitive poly(N,N-dimethylaminoethyl methacrylate) hydrogels prepared with different crosslinking agents. Polym Eng Sci. 2013;53(4):734–43. doi:10.1002/pen.23308.
39. Thakur S, Arotiba OA. Synthesis, swelling and adsorption studies of a pH-responsive sodium alginate-poly(acrylic acid) superabsorbent hydrogel. Polym Bull. 2018;75(10):4587–606. doi:10.1007/s00289-018-2287-0.
40. Hu X, Yan L, Wang Y, Xv M. Self-assembly of binary oppositely charged polysaccharides into polyelectrolyte complex hydrogel film for facile and efficient Pb^{2+} removal. Chem Eng J. 2020;388:124189. doi:10.1016/j.cej.2020.124189.

41. Song Z, Liu X, Ding J, Liu J, Han X, Deng Y, et al. Poly(acrylic acid)-based composite gel polymer electrolytes with high mechanical strength and ionic conductivity toward flexible zinc-air batteries with long cycling lifetime. ACS Appl Mater Interfaces. 2022;14(44):49801–10. doi:10.1021/acsami.2c14470.
42. Chaudhuri SD, Mandal A, Dey A, Chakrabarty D. Tuning the swelling and rheological attributes of bentonite clay modified starch grafted polyacrylic acid based hydrogel. Appl Clay Sci. 2020;185(9):105405. doi:10.1016/j.clay.2019.105405.
43. Zhang SW, Han DD, Ding ZX, Wang X, Zhao D, Hu Y, et al. Fabrication and characterization of one interpenetrating network hydrogel based on sodium alginate and polyvinyl alcohol. J Wuhan Univ Technol. 2019;34(3):744–51. doi:10.1007/s11595-019-2112-0.
44. Hu O, Lu J, Chen G, Chen K, Gu J, Weng S, et al. An antifreezing, tough, rehydratable, and thermoplastic poly(vinyl alcohol)/sodium alginate/poly(ethylene glycol) organohydrogel electrolyte for flexible supercapacitors. ACS Sustain Chem Eng. 2021;9(29):9833–45. doi:10.1021/acssuschemeng.1c02464.
45. Adelnia H, Ensandoost R, Moonshi SS, Gavgani JN, Vasafi EI, Ta HT. Freeze/thawed polyvinyl alcohol hydrogels: present, past and future. Eur Polym J. 2022;164(11):110974. doi:10.1016/j.eurpolymj.2021.110974.
46. Cao C, Li Y. Highly stretchable calcium ion/polyacrylic acid hydrogel prepared by freezing-thawing. J Mater Sci. 2020;55(12):5340–48. doi:10.1007/s10853-019-04332-8.
47. Park E, Ryu JH, Lee D, Lee H. Freeze-thawing-induced macroporous catechol hydrogels with shape recovery and sponge-like properties. ACS Biomater Sci Eng. 2021;7(9):4318–29. doi:10.1021/acsbiomaterials.0c01767.
48. Naeem A, Yu C, Zhu W, Zhu W, Wu X, Chen L, et al. Gallic acid-loaded sodium alginate-based (poly-vinyl alcohol-co-acrylic acid) hydrogel membranes for cutaneous wound healing: synthesis and characterization. Molecules. 2022;27(23):8397. doi:10.3390/molecules27238397.
49. Kowalski G, Witczak M, Kuterasiński Ł. Structure effects on swelling properties of hydrogels based on sodium alginate and acrylic polymers. Molecules. 2024;29(9):1937. doi:10.3390/molecules29091937.
50. Liu X, Wu Z, Jiang D, Guo N, Wang Y, Ding T, et al. A highly stretchable, sensing durability, transparent, and environmentally stable ion conducting hydrogel strain sensor built by interpenetrating Ca^{2+}-SA and glycerol-PVA double physically cross-linked networks. Adv Compos Hybrid Mater. 2022;5(3):1712–29. doi:10.1007/s42114-021-00396-w.
51. Mandal B, Ray SK. Synthesis of interpenetrating network hydrogel from poly(acrylic acid-co-hydroxyethyl methacrylate) and sodium alginate: modeling and kinetics study for removal of synthetic dyes from water. Carbohydr Polym. 2013;98(1):257–69. doi:10.1016/j.carbpol.2013.05.093.
52. Bardajee GR, Mahmoodian H, Boraghi SA, Elmizadeh H, Ziarani NB, Rezanejad Z, et al. Nanoporous hydrogel absorbent based on salep: swelling behavior and methyl orange adsorption capacity. Environ Res. 2023;225:115571. doi:10.1016/j.envres.2023.115571.
53. Tan J, Luo Y, Guo Y, Zhou Y, Liao X, Li D, et al. Development of alginate-based hydrogels: crosslinking strategies and biomedical applications. Int J Biol Macromol. 2023;239(1):124275. doi:10.1016/j.ijbiomac.2023.124275.
54. Lv H, Zong S, Li T, Zhao Q, Xu Z, Duan J. Room temperature Ca^{2+}-initiated free radical polymerization for the preparation of conductive, adhesive, anti-freezing and UV-blocking hydrogels for monitoring human movement. ACS Omega. 2023;8(10):9434–44. doi:10.1021/acsomega.2c08097.
55. Zhou B, Kang W, Jiang H, Yang H, Li Z, Lv Z, et al. Preparation and crosslinking mechanism of delayed swelling double-crosslinking nano polymer gel microsphere for anti-CO_2 gas channeling. J Pet Sci Eng. 2022;219(10):111122. doi:10.1016/j.petrol.2022.111122.
56. Mahinroosta M, Farsangi ZJ, Allahverdi A, Shakoori Z. Hydrogels as intelligent materials: a brief review of synthesis, properties and applications. Mater Today Chem. 2018;8(2):42–55. doi:10.1016/j.mtchem.2018.02.004.
57. Kang M, Cheng Y, Hu Y, Ding H, Yang H, Wei Y, et al. Self-healing poly(acrylic acid) hydrogels fabricated by hydrogen bonding and Fe^{3+} ion cross-linking for cartilage tissue engineering. Front Mater Sci. 2023;17(3):230655. doi:10.1007/s11706-023-0655-7.
58. Gao B, Yu H, Wen J, Zeng H, Liang T, Zuo F, et al. Super-adsorbent poly(acrylic acid)/laponite hydrogel with ultrahigh mechanical property for adsorption of methylene blue. J Environ Chem Eng. 2021;9(6):106346. doi:10.1016/j.jece.2021.106346.

59. Malatji N, Makhado E, Modibane KD, Ramohlola KE, Maponya TC, Monama GR, et al. Removal of methylene blue from wastewater using hydrogel nanocomposites: a review. Nanomater Nanotechnol. 2021;11:18479804211039425. doi:10.1177/18479804211039425.
60. Li Z, Lin Z. Recent advances in polysaccharide-based hydrogels for synthesis and applications. Aggregate. 2021;2(2):21–46. doi:10.1002/agt2.21.
61. Elaf R, Ali AB, Saad M, Hussein IA, Bai B. Development of eco-friendly chitosan-g-polyacrylamide preformed particle gel for conformance control in high-temperature and high-salinity reservoirs. Geoenergy Sci Eng. 2023;230(1):212136. doi:10.1016/j.geoen.2023.212136.
62. Liu Y, Zheng Y, Wang A. Response surface methodology for optimizing adsorption process parameters for methylene blue removal by a hydrogel composite. Adsorpt Sci Technol. 2010;28(10):913–22. doi:10.1260/0263-6174.28.10.913.
63. Sabbagh F, Muhamad II, Nazari Z, Mobini P, Taraghdari SB. From formulation of acrylamide-based hydrogels to their optimization for drug release using response surface methodology. Mater Sci Eng C. 2018;92:20–5. doi:10.1016/j.msec.2018.06.022.
64. Zheng Y, Liu Y, Wang A. Fast removal of ammonium ion using a hydrogel optimized with response surface methodology. Chem Eng J. 2011;171(3):1201–8. doi:10.1016/j.cej.2011.05.026.
65. Mohtaram MS, Sabbaghi S, Rasouli J, Rasouli K. Photocatalytic degradation of tetracycline using a novel WO_3-ZnO/AC under visible light irradiation: optimization of effective factors by RSM-CCD. Environ Pollut. 2024;347(12):123746. doi:10.1016/j.envpol.2024.123746.
66. Zhou Z, Chen S, Han Z, Qu X, Deng L, Song J, et al. Continuous preparation of the record strength and toughness hydrogel fibers with a homogeneous crosslinked network by microcrystalline dispersed growth. Adv Funct Mater. 2024:2415354. doi:10.1002/adfm.202415354.
67. Zhao Z, Shen Y, Liu Y, Wang J, Ma M, Pan J, et al. Investigation of silicon doped carbon dots/carboxymethyl cellulose gel platform with tunable afterglow and dynamic multistage anticounterfeiting. J Colloid Interface Sci. 2024;672(18):142–51. doi:10.1016/j.jcis.2024.05.227.
68. Van TN, Quang TD, Hung TT, Xuan QC, Van TH, Kim H, et al. Enhancing mechanical properties of polyvinyl alcohol/sodium alginate gel beads by graphene oxide for the aerobic sludge immobilization in wastewater treatment. Environ Eng Res. 2023;28(5):220403. doi:10.4491/eer.2022.403.